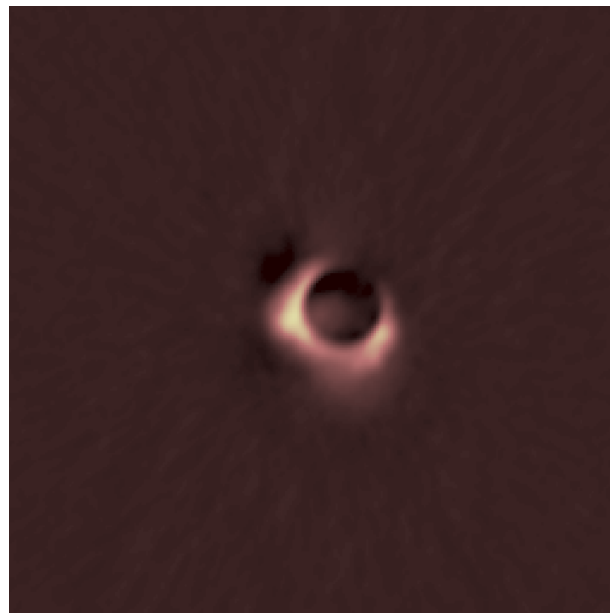




Universiteit Leiden

Radio Astronomy

The solar eclipse of 2015 as seen by LOFAR



Authors:

Margherita Grespan (s2233150)
Ioannis Politopoulos (s2304090)

1 Introduction

LOFAR (Low Frequency Array) is radio frequency telescope array, built and operated by ASTRON, Netherlands, and was designed for low radio frequency (<250MHz) observations. It consists of a core located in the Netherlands with its longest baseline being 100 km. Nowadays, it expands all around Europe with the LOFAR International program with the longest baseline extending up to 1500 km. The variety of applications for such telescope are immense.

Various phenomena that happen to the Sun can be observed in low frequency radio waves. The outer “atmosphere” of the Sun, the corona, can be effectively considered as a bright radio source. Numerous phenomena that happen to the corona are visible in the radio frequency and are observed by LOFAR (in 110-190 MHz range). One event of particular interest is the solar eclipse. Such an event happened in March 20, 2015. While it was a total solar eclipse in some countries, in the Netherlands it was only a partial eclipse with a maximum of $\approx 85\%$ Sun obscuration and was observed by the LOFAR core.

In this document we describe the calibration and imaging process of the observation. The expected brightness of the Sun, the thermal noise and the Moon are calculated, the data reduction is described, different methods are analyzed and finally we show the resulting images of the eclipse.

1.1 The Dataset and Expected Results

In this section, we will show a brief analysis for the expected values of important parameters for our observations, such as the expected signal and noise, the necessary calculations for the required resolution. The assumption taken are demonstrated to ensure the imaging - with this observation - is valid. Finally, we show the dataset used.

From the antennas configuration shown in Figure 1 is it possible to derive the maximum baseline, hence resolution of the observation.

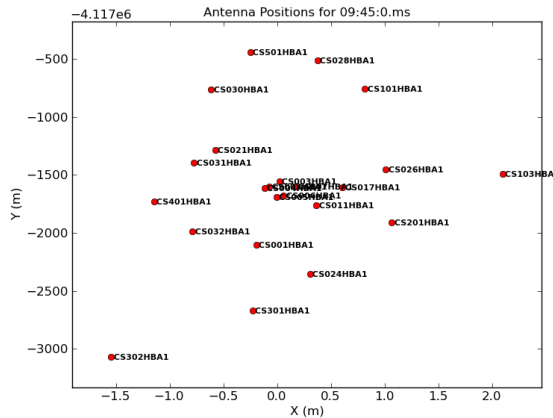


Figure 1: The antenna positions for the 9:45 observation. We assume the position does not change for the other datasets.

$$\text{resolution(radian)} \approx (\text{observed wavelength}) / (\text{length of longest baseline}) \approx \lambda/B \quad (1)$$

As mentioned, the observations are in a range of 110-190 MHz, taking the median, $\nu = 150\text{MHz}$ which is an observed wavelength of ≈ 2 m.

From Figure 1 we check the position of the farthest apart antennas and in the `listobs` we find their x,y position which gives longest baseline = 3446.533 m = 1723.267 λ . Therefore, angular resolution = 1.995 arcmin \approx 2 arcmin.

For our sampling, we need to consider the *Nyquist Sampling theorem* which states that we are required to sample at least twice per resolution element to adequately sample our source with said resolution. Therefore, our pixel size shall be 1/2 of the resolution element, which results in a cell size (see `tclean` parameters in sec. 2.1) of 1 arcmin.

In addition to the resolution, the amount of pixels to calculate the primary beam needs to be calculated. Since the Sun in radio has an angular diameter of $\approx 1\text{deg}$, to safely include the Moon and the Sun in our image (if for any reason it is not perfectly centered), we would require our image size to be 4-5 times of the Sun diameter. Using 256 pixels gives us $256 \text{ arcmin} = 4.27\text{deg}$ which satisfies our criterion.

To later confirm whether our calibration is within reason, it is useful to calculate the expected brightness of the Sun. A logical assumption would be to consider the Sun's corona to be 10^6K [1]. Using the Planck's (Black Body) Law for this given temperature, a central frequency of 150 MHz and in a range of 110-190 MHz, we can calculate the spectral radiance. However, we need to consider the angular size of the Sun, which in our case is considered to be ≈ 15 arcmin. Combining the above, we calculate the expected signal from the Sun to be:

$$S_{\odot} = 4.1 \cdot 10^4 \text{Jy} \quad (2)$$

Our main natural noise source (so not interference from man-made devices), will be the thermal noise from the atmosphere. Assuming that the atmosphere has a mean temperature of $\approx 300\text{K}$, for the same central frequency and range, and for a patch of sky of the same dimensions as the Sun, we can calculate:

$$S_{\text{Thermal Noise}} = 12.38 \text{Jy} \quad (3)$$

Actually, the resulting noise will be slightly higher because the source is not in the far field so Fresnel propagation shall be considered, but it will be in same the order of magnitude nevertheless.

Similarly, assuming the diameter of the Moon to be equal to the Sun's (this assumption is held because we know that this was a total solar eclipse in other regions of the Earth) and a Moon's temperature of 15 K, we can calculate the expected signal from the Moon.

$$S_{\text{Moon}} = 6.19 \text{Jy} \quad (4)$$

Knowing that the Moon is darker than the thermal noise of the surrounding area around the Sun, means that one could calculate the exact position of the Moon on sky and measure the brightness at that position. Afterwards, calibrating for the Moon as a source (for which we know the absolute brightness), we can safely assume that the absolute brightness of the diffuse emission is the residual of the calibration at that position.

To confirm whether the Sun is sufficiently far away to consider planar waves, we are required to calculate the Fraunhofer distance for our current baseline. The longest baseline for our central frequency of 150MHz, is 1723.267λ

$$\text{Near Field} < \frac{2D^2}{\lambda} = 1.188 \cdot 10^4 \text{ km} \quad (5)$$

But 1 AU $\approx 1.496 \cdot 10^8$, so the Sun is confidently in the far field and it is safe to consider planar waves. Similarly, we can calculate the Fraunhofer distance for the shortest observed wavelength for the LOFAR-NL core and for the international LOFAR array. The shortest wavelength is $\lambda_{\min} = 1.5779\text{m}$ (190MHz).

LOFAR-NL core: Longest Baseline = $2184.254\lambda_{min}$

$$FraunhoferDistance = \frac{2D^2}{\lambda_{min}} \approx 1.506 \cdot 10^4 \text{ km} \quad (6)$$

LOFAR International: Longest Baseline = $1900 \text{ km} = 1.204 \cdot 10^6 \lambda_{min}$

$$FraunhoferDistance = \frac{2D^2}{\lambda_{min}} \approx 4.576 \cdot 10^9 \text{ km} \quad (7)$$

But $1 \text{ AU} \approx 1.496 \cdot 10^8$, so if we had observations using the international LOFAR array, we would have to consider Fresnel propagation of the waves.

One more consideration we need to take into account for our imaging, is the relative motion of the Sun and the Moon with respect to the “J2000” coordinate system that LOFAR is tracking. This will determine the required integration time of the observations.

The on sky velocities of the Moon and Sun are equal to $\approx 0.5 \text{ deg/hour}$ and $\approx 15 \text{ deg/hour}$ correspondingly. The relative movement of the Moon with respect to the Sun is equal to $\approx 14.5 \text{ arcsec/sec}$. This means that in 4 seconds the Moon moves on sky by 58 arcsec. However, the minimum resolution for our baseline for the 150MHz frequency is 1 arcmin. So we conclude that at an at least 5 sec integration time is required to adequately sample the movement of the Moon on sky with our current setup. For a 5 sec integration time, the movement of Moon on sky in respect to the Sun is 1.21 arcmin which is within our resolution.

1.2 The dataset

Throughout this work we use LOFAR data of the total solar eclipse that took place on March 20th, 2015 (Project code: DDT3_003).

The data have been reduced with the use of the Common Astronomy Software Applications - CASA¹ [2] software version 5.6.0.

The data were recorded with all the baselines (23 antennas) between half of the LOFAR core’s HBA² antenna fields. Hence, the dataset constitutes of sub bands of the spectra range between 110 and 190 MHz with - between 07:25 and 11:55 UTC - 5 seconds of observation time every 5 minutes.

To proceed with the investigation of the data it is necessary to merge the sub bands - in each 5 seconds observation - which are otherwise scattered in the spectrum field. This can be done with the CASA command `concat`. If some data are corrupted the run of this command will be interrupted, we can discard the datasets in which this happens.

2 Data reduction

In this section, we discuss the data reduction of the dataset, explain the calibration and cleaning process and analyze the methods used.

¹<https://casa.nrao.edu/>

²High Band Antenna which is optimized for 120-240 MHz

Firstly, we inspect the uv-coverage. With an observation time of 5 seconds (almost a snapshot) we expect a quite poor uv-coverage, such as the one shown In Figure 2 (Left). We can see that 5 seconds of observation is not enough to populate the uv plane using the antennas shown in Figure 1 and exploiting the Earth rotation. However, in the same set of observations, we found some sets of data with significantly worse uv-coverage, such as the one shown in Figure 2 (Right). In our study, we discard the latter datasets. The cause of this may be a corrupted file, an error while downloading the file or a variety of other errors in earlier stages of the process. (The problem persisted even after re-downloading the data)

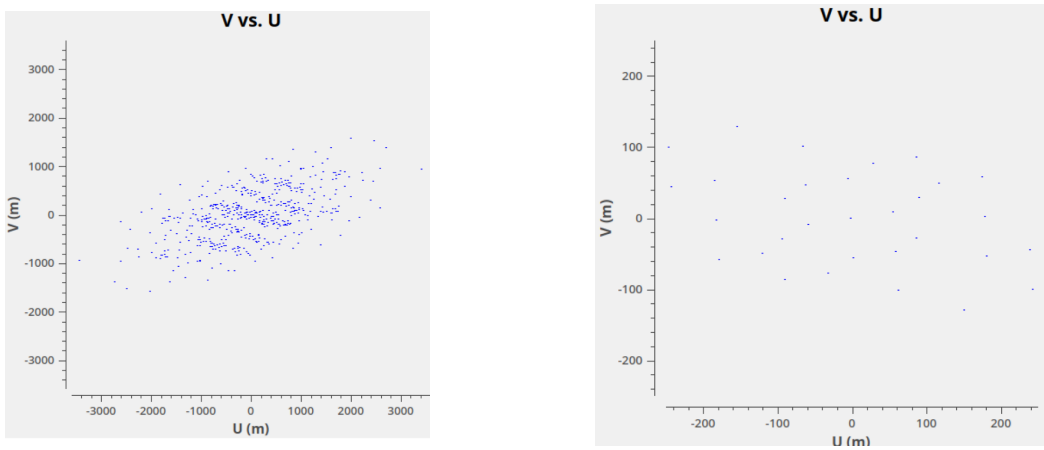


Figure 2: Left: UV coverage of the observation. Right: Example of poor UV coverage for a discarded dataset (09:20:00).

Bandpass Calibration

We start with the external, or *a-priori*, calibration. This makes use of known sources, called calibrators, in order to correct the data. Calibrators are bright and isolated sources whose position and intensity are known. In our dataset a calibration table of the source Cygnus A was given. Meaning that a model was created on previous observations of the radio galaxy Cygnus A.

The first step of this calibration is focused on fixing instrumental effects and variations *vs* frequency. this is called bandpass calibration and corrects the frequency-dependent part of the gains. The bandpass, is a filter used in radio telescopes, which passes the wanted range of frequencies and attenuates those outside of it. Having the bandpass calibration table, allows us to apply it to every observation in the dataset, more precisely, this is done with the CASA command `applycal`.

Manual Flagging

After applying our first calibration we shall proceed to manual flagging. The CASA command `plotms` permits to plot an `.ms` file, namely the files we previously concatenated and for each, we plot the frequency *vs* amplitude. As is demonstrated in Figure 3, due to the interference of different antenna signals, some channels have increased amplitude. We suspect certain channels mostly affected due to Radio Frequency Interference (**RFI**). Another cause of this may be radio waves of other nearby (terrestrial) sources which emit at similar frequencies (this frequency range being rather busy).

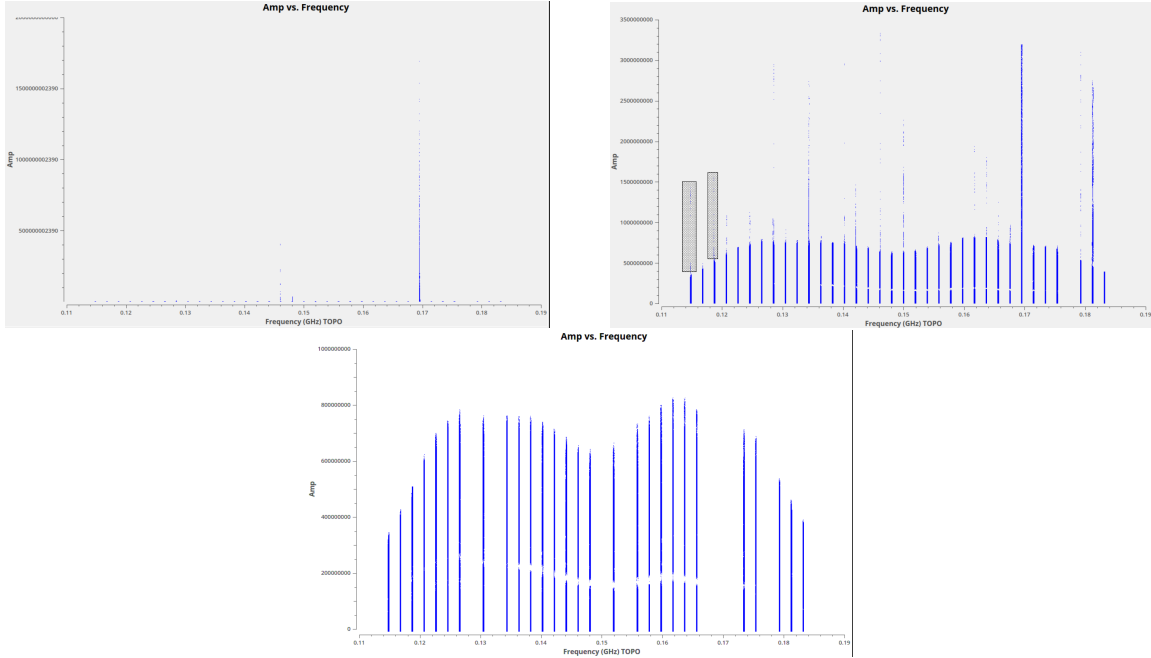


Figure 3: Amplitude vs Frequency of our dataset (11:35:00) **Top Left:** Before flagging **Top Right:** in the process of flagging, **Bottom:** After flagging.

2.1 Cleaning – Stokes I calibration

To reconstruct an image of the sky from the interferometer response, we have to compute the Fourier transform of the visibility. In CASA this is done using the task `tclean`, which also performs the image deconvolution. This command permits to iteratively adapt a mask on the detected sources and enhance the signal that comes from those in respect to the background noise.

In order to retrieve the best signal to noise ratio and detect the kind of source that we are interested in (i.e. small or extended sources) it is important to tune the correct parameters in `tclean`. Some of the parameters tuned are the following (the value used are in tab.1):

- **imsize:** Number of pixels in the image (size of the image).
- **cell:** size of the cell. See subsec. 1.1 for the mathematical derivation of this value.
- **deconvolver:** Deconvolution is the process of reconstructing a model of the sky brightness distribution given a dirty/residual image and the point-spread-function of the instrument. Deconvolution in CASA is made through minor cycles of image reconstruction that can be done in different ways. One option is mtmfs a.k.a. Multi-term (Multi Scale) Multi-Frequency Synthesis [3]. The multi-scale is used to have a scale sensitive deconvolution and properly deconvolve complicated structures. In our case the Sun, as seen from the Earth, assumes different shapes when occulted by the Moon so this approach is essential. The multi-frequency is used to model wide-band brightness of the sky. This deconvolution type requires `nterms` greater than 1.
- **scales:** Scales of the possible sources in the image at which the image has to be deconvolved.
- **stokes:** Stokes Planes to image.

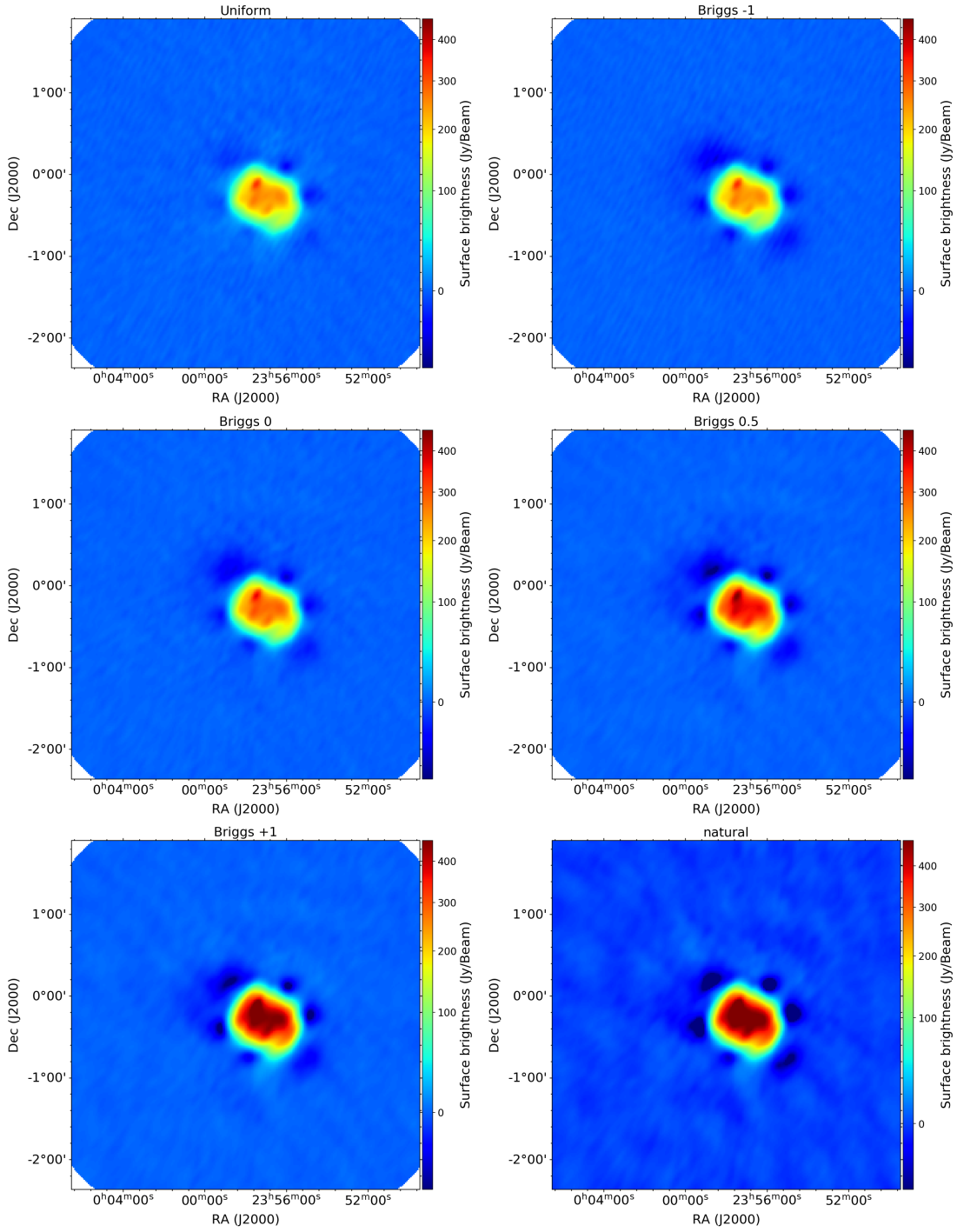


Figure 4: Different weighting applied to the 7:50 dataset. The images have the same colorscale. We picked as minimum (maximum) pixel value the minimum (maximum) value in this set of images.

Table 1: `tclean` parameters.

imsize	cell	deconvolver	scales	stokes	weighting	nterms	gridded	wpp
1 arcmin	256	mtmfs	[0,1,2,4,8,16,32,64]	I	briggs	3	wproject	-1

- **weighting**: the type of weighting scheme to apply to visibilities. The weighting scheme applied to the data determines which spatial scales are weighted more when imaging. The available options of weighting schemes are:

- Natural: Each sample is given the same weight. Will give the largest beam and the best surface brightness sensitivity. Best for extended objects.
- Uniform: Each visibility is given a weight inversely proportional to the sample density. The result will be to have the long baselines more pronounced which enhances the resolution. However, it has poorer noise characteristics.
- Briggs: It is a compromise between the uniform and the natural weighting which is tuned using the `robust` parameter. This permits to transit from a Natural weight (`robust= -2`) to an uniform (`robust= 2`). Hence, in order to have an intermediate response to the signal a value around 0 of the `robust` is used.

To show the effect of the weighting scheme we the 7:55 observation is imaged with different schemes, Figure 4. With a uniform weighting, the edges of the Sun are resolved but the flux is not as high as in the natural weighting. The images with an increasing `robust` value clearly show how this value affects the imaging. Going from uniform to natural the flux of the Sun increases but at the same time some artifacts/dark blobs around the edge of the source appear. With a source as bright as the Sun, the signal level is not a problem but big artifacts like the dark blobs, are. For this reason, we decided to image the eclipse with Briggs and `robust=-1`.

- **nterms**: Number of Taylor coefficients to model the sky frequency dependence. The higher is the amount of nterms the finer features can be taken into account in the cleaning model we are creating. Thus, the increase of terms approximation terms increases the running time in CASA and can also lead to overfitting. In Figure 5 is shown the difference between an image with 2 and 4 `nterms`. With 2 terms we have more noise around the Sun, so an higher amount of Taylor coefficients is needed. Thus, comparing Figures 4 and 5 we do not spot great differences in an image with 3 or 4 `nterms` hence we will use the former since it requires less computational time.
- **gridded**: Deconvolution grid. `projectplanes` is one kind of gridding which samples the w plane. It is needed when having a wide field.
- **wprojectplanes**: The amount of project planes to sample. This value can be calculated knowing the size of the detected object and cells used in the imaging. However `tclean` accepts the value -1 which automatically calculatew the amount pf project planes needed for the imaging. This can be used only when the source is clearly visible in respect to the noise level which satisfied in our case.

Cleaning is the process of creating a model of the source which - in CASA - is saved in the model column of the `.ms` file, extrapolated by `gaintcal` and therefore saved as a calibration table. The calibration table is then applied - together with the bandpass - to the corrected column by the `applycal` task. For the last step of the imaging process, when a model of the source is used to calibrate the source itself, is also called **self-calibration**.

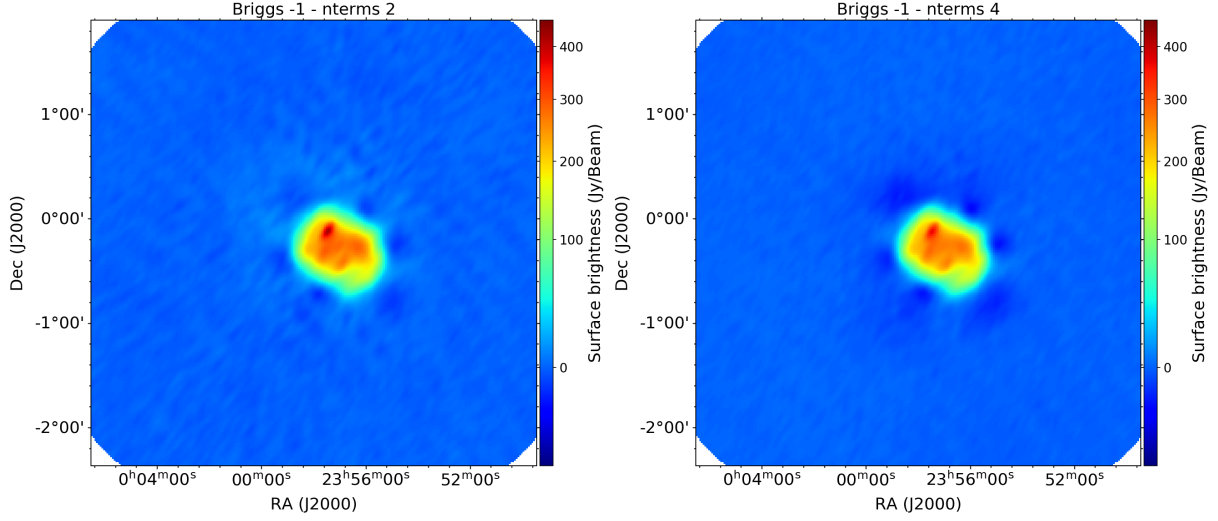


Figure 5: Images of the 7:50 dataset with different nterms.

Gaincal includes choosing between “phase only”, “amplitude and phase” or “amplitude” only calibration. For the first couple of iterations, “phase only” calibrations are required to pinpoint the location of the source and hence focus our calibration on the part of the image where the Sun is. However, the phase calibrations are usually not enough to retrieve a high sensitivity on the image and increase the detected flux. For this reason, after two “phase only” calibrations are completed, two “amplitude and phase” calibrations are done to calibrate for the shape and the amplitude of the wavefront of our source. The process to improve the source model is the same as the previous iterations, the only difference now is that we are also finding the amplitude correction factors. If the noise level is within our requirement, the final image (line 127-142 in the code in Appendix B) of a single configuration is ready.

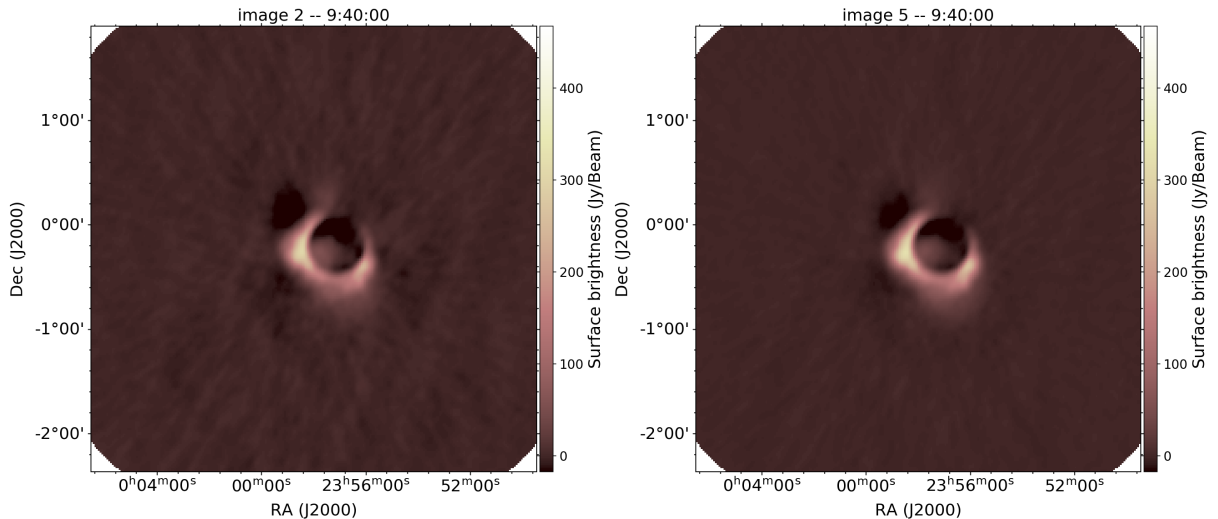


Figure 6: Image with 1 phase calibration only vs image with 2 rounds of phase calibration and 2 of phase and amplitude

2.2 Polarization Calibration

To detect polarization LOFAR, has wire dipoles sensitive to 2-orthogonal linear polarisations. The signal collected by the antenna is divided in X-Y components (two orthogonal polarization states) by the the antenna polarizer. In order to not mix the polarization components contributions, at the LOFAR station, the two signals travel through essentially independent paths until the correlator. However, the instrument is not ideal - mechanical imperfection in the feed or electronics will always be present - and this causes leakage of one into the other at various points in the signal chain. To make things worse, the LOFAR antennas are stationary on the ground and this will affect the polarization because the antennas can not track the sky leading to a projection of the dipoles when they are not looking at the zenith. Futhermore, this causes variations in the antenna's polarization response and therefore leakage which is of the order of tens of percents [4]. Polarization leakage gives rise to spurious linear polarization, biased visibility amplitudes and phases. Anyway, the polarization response does not changes a lot across the field of view of an HBA station, this makes the polarimetry with the HBA easier [4].

In order to correct for the leakage, we create a model on the most updated Stokes I image of the Sun. This is done with the `polcal` task which takes as an input the visibility file and gives the polarization calibration table as output. The type of polarization solution (poltype) is also requested. We solved only for instrumental polarization (Df).

Finally the polarization calibration table is applied with `applycal` together with the latest self calibration table and the latest phase only self calibration table and bandpass calibration.

3 Results

Three images are of particular interest, namely, the observations at 9:30:00, 9:40:00 and 11:55:00. This is because these images show an interesting phenomenon in 9:30:00, an observation close to the maximum eclipse in 9:40:00 and the Sun close to its maximum elevation. These images will be further discussed in Section 4. Some analysis was done for these images and is presented below.

3.1 Cleaning results

Using a mask within each iteration of the cleaning process, we can extract some statistics for each image. Of great importance for comparison, are the **RMS** of the noise around the Sun and the **brightness** of the Sun itself. These values are shown in Table 2 (for some images we could not extract the Flux of the Sun from the IQUV image, fot this reason there are missing data on the table. However the trend is still visible). Using the data obtained, to visualize and show the effect of our cleaning process, in Figure 7 the RMS and Brightness per selfcal iteration is demonstrated. Moreover, Figure 9 shows how self calibration and the final `polcal` calibrates the gain range (y-axis range decreases).

3.2 Polarization

In Sec. 2.2 we discussed why a calibration polarization is needed. In Figures 10 and 11 we show the results of this approach for before and after the polarization calibration respectively.

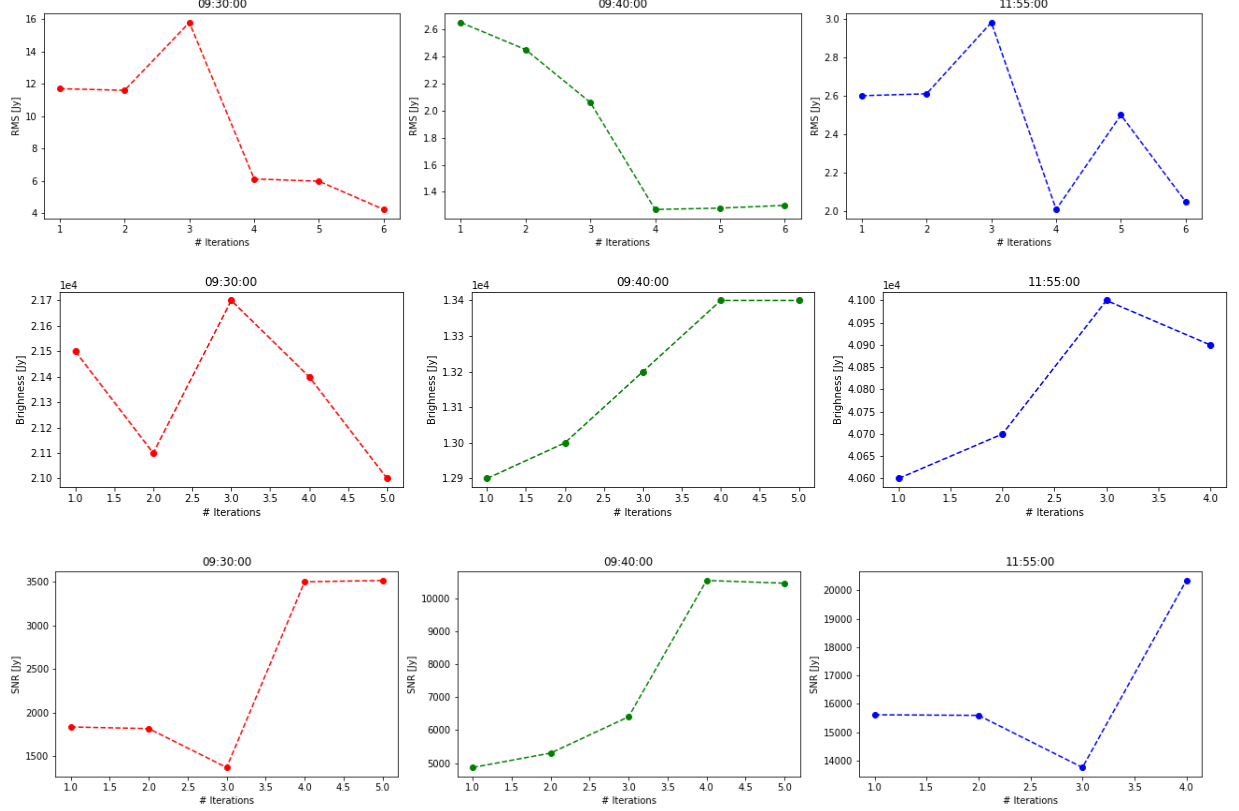


Figure 7: Top: RMS vs Selfcal Iteration. Middle: Brightness vs Selfcal Iteration. Bottom: SNR vs Selfcal Iteration.

Table 2: Statistics of the images.

image	type calibration	09:30		09:40		11:55	
		RMS Background	Flux Sun	RMS Background	Flux Sun	RMS Background	Flux Sun
1	phase	1.17e1	2.15e4	2.65	1.29e4	2.60	4.06e4
2	phase	1.16e1	2.11e4	2.45	1.30e4	2.61	4.07e4
3	amp +phase	1.58e1	2.17e4	2.06	1.32e4	2.98	4.10e4
4	amp +phase	6.11	2.14e4	1.27	1.34e4	2.01	4.09e4
5	amp +phase	5.97	2.10e4	1.28	1.34e4	2.5	
6	polcal+amp+phase	4.22		1.20		2.05	

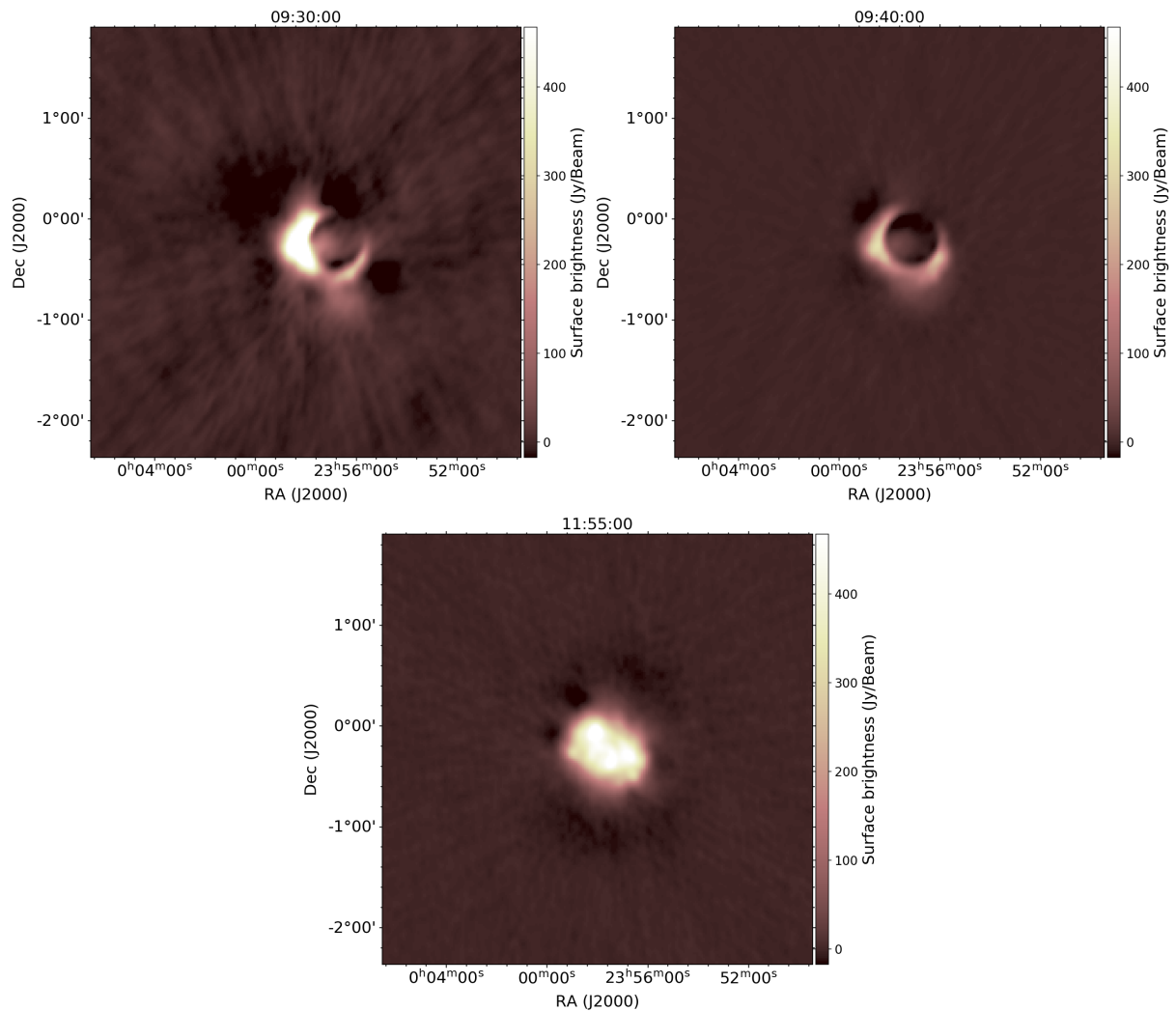


Figure 8: Required images polarization corrected.

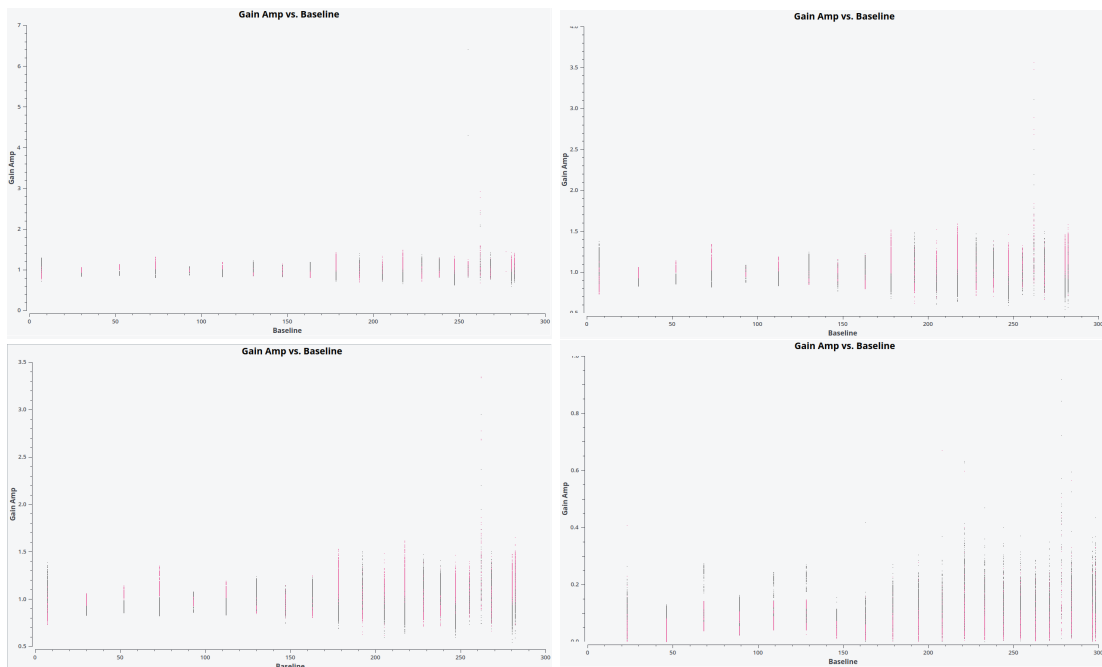


Figure 9: Baseline vs Gain Amplitude for the 11:55 self calibration tables. **Top left:** selfcal n. 3 this calibration table is the first one created with a phase and amplitude calibration. It has the highest gain values. , **Top right:** selfcal n. 4 the gain amplitude is lower. **Bottom left:** selfcal n. 5. The gain amplitude does not show big changes from the previous calibration table. The longest baselines have the highest Gain. **Bottom right:** polarization calibration. The Gain Amplitude is incredibly reduced.

The axis upon which the plotted points are colorized, is the correlation.

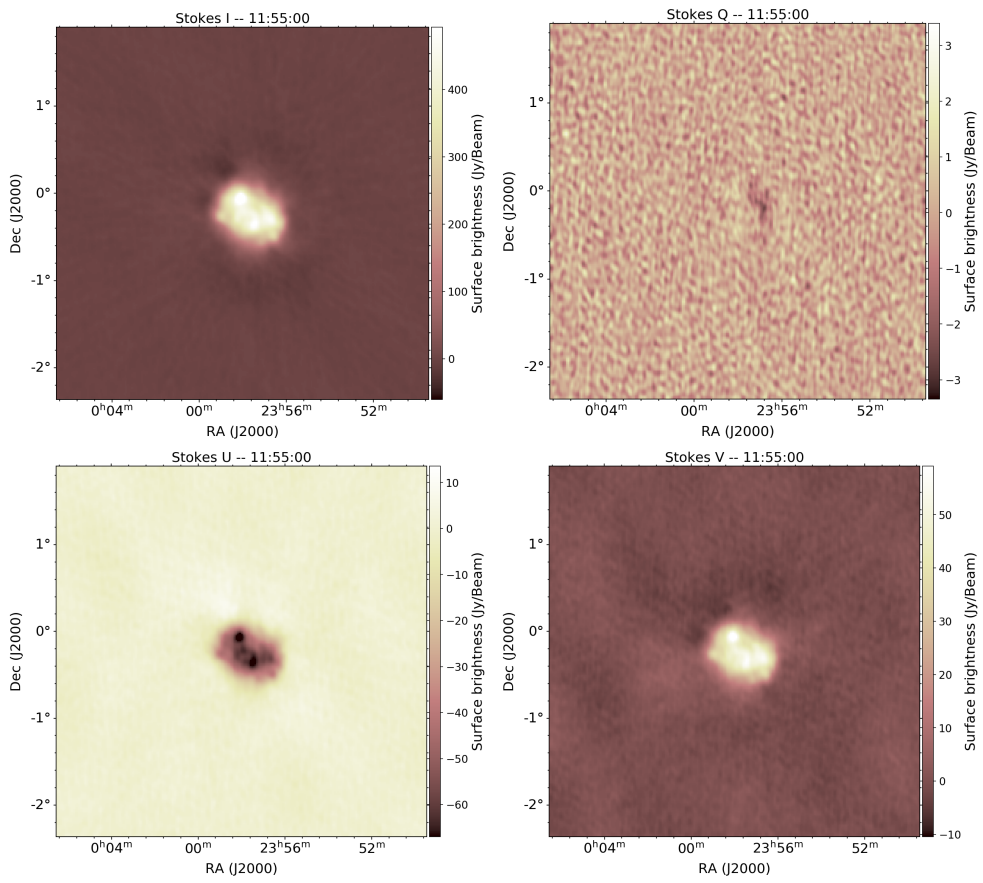


Figure 10: Images for the I, Q, U and V polarizations from left to right, before the polarization calibration.

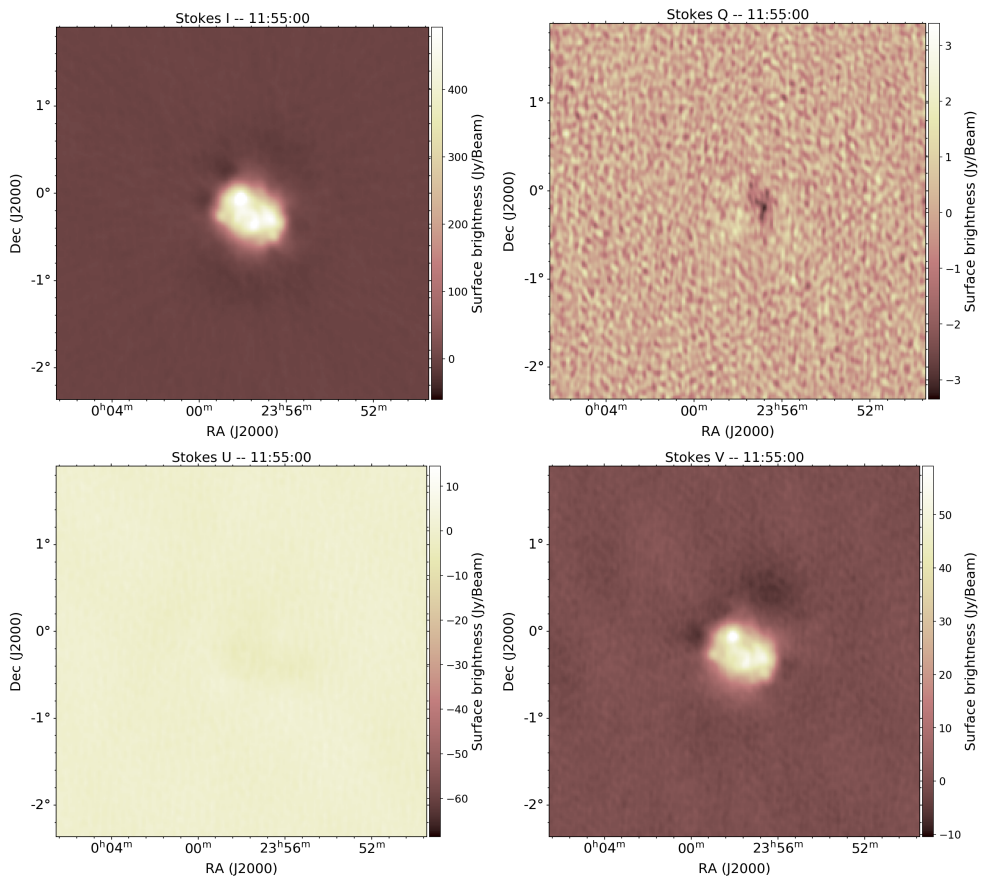


Figure 11: Images for the I, Q, U and V polarizations from left to right, after the polarization calibration.

4 Discussion

In this section, we will discuss about the resulting images after the cleaning process is complete, shown in Figure 8, and some points of interest. Three images are of particular interest, namely, the observations at 9:30:00, 9:40:00 and 11:55:00.

The 9:30:00 observation is special, because a bright spot from within the Sun is occulted by the Moon. However, mountains on the Moon highly diffract the observed wavelengths. The result of this diffraction is to be seen as a new source, which lies much closer than the Sun for which our calibration is done. In this observation, this diffraction will be greatly enhanced when compared to other observation times such as the 9:40:00 because the source of the diffraction is the aforementioned active region. This will result in a much noisier image of the Sun (top left plot in Figure 7). Additionally, we can see that more structures are visible “outside” of the Sun and this is because of the bright “edges” like the one the diffraction creates, produced increased imaging errors which appear as artifacts similar to the black blobs around the Sun or the radial structure that is visible in this observation after cleaning. To further support our claim, these artifacts are not visible in the other two observations that do not contain such strong flux differences.

9:40:00 is also of special interest since it is close to the maximum eclipse which occurs at 9:46:47. One thing to notice in this observation, is that within the Moon, the flux and noise are significantly reduced, because the Moon is darker than the surrounding atmosphere. However, due to the preceding diffraction described in observation 9:30:00, there is some flux which falsely appears to be within the Moon.

Other pictures, of less interest, are shown in the Appendix A without further explanation.

Finally, 11:55:00 is also important because the Sun is close to its maximum elevation and the Moon is not visible. To confirm that the Moon is not visible, we can consider the relative motion of the Sun and the Moon. In Subsec. 1.1 we showed that the relative velocity of the Moon and the Sun is 14 arcmin/min. Which means that from 9:40:00 until 11:55:00, 135 minutes have passed which correspond to the Moon moving by 1957.5 arcmins = 32.625 degrees which is confidently far away from our field of view of 4.27 deg around the Sun. The aforementioned images are shown in Figure 8.

Finally, to comprehensively calibrate the diffraction originated from the mountains of the lunar surface, we should take into account that the diffraction from the two sides of the same mountain are correlated and therefore will invalidate the van Cittert Zernike theorem. This means that in the interference pattern on the ground carries information about the lunar surface and the edge of the disk as seen by LOFAR. Specifically, the direction of the fringes will follow a theoretical line that connects the two “holes” that produce the fringes which in our case are the two sides of the lunar mountain, much like the double slit experiment. The amplitude of these fringes can also be calculated via the same method. Overall, this effect can be calculated and calibrated out. (For the extra “bonus” challenge II)

The results of our cleaning process displayed in figure 7 and Table 2, indicate a significantly reduced RMS for the sky surrounding the Sun. The resulting RMS matches well with the predicted thermal noise in Equation 3 before the cleaning and is properly corrected. Additionally, our resulting flux for the unocculted Sun, hence the 11:55 observation, of $4.09 \cdot 10^4 Jy$ also matches well with our previous calculation in Equation 2 of $4.1 \cdot 10^4 Jy$.

When deciding for the weighting (Figure 4) we evidenced the presence of black blobs - negative fluxes - around to the Sun’s edge. Encountering sharp brightness gradient the cleaning algorithm creates these artifacts. This is particularly visible in the 9:30:00 observation in which the bright spot is barely occulted and increases the noise as described.

Figure 7 and 9, demonstrated the efficiency of the calibration table for the noise reduction. Even if we create a model on a Stokes I source, this enable us to reduce the noise and enhance the signal to noise ratio. In Figure 6 the image two phase only and two phase and amplitude calibrations of the 9:40 dataset is displayed. This is the image before the polarization calibration table is applied. In Figure 8 we show

the image after the polarization calibration. Comparing the Figures 8 and 6, one cannot see a visible significant increase in the signal to noise ratio but it is reflected in the RMS decrease in Figure 7. Since the difference is not visible, we consider showing the images for the other two required times (9:30 and 11:55) not of great importance, however they are available if requested.

To demonstrate the improvement of the image after the polarization calibration, we considered fitting to use the 11:55:00 dataset and is more intuitive to describe and visualize. This demonstration is shown in Figures 10 and 11 for before and after the calibration respectively. As referenced in 2.2, LOFAR detects only linear polarization and because of this, the polarization calibration for the V stokes (circular polarization) does not yield an accurate result. The Stokes Q - diagonal polarization - does not change after calibration and finally, Stokes U has been efficiently calibrated.

5 Conclusions

In summary, throughout this work, we show the calibration and imaging of the 2015 solar eclipse as seen by LOFAR. The required cleaned images are displayed in Figure 8 and the additional observations used to create a movie of the eclipse in the Appendix A (Figures 12 and 13). Using the entirety of the final images, we created a short movie that can be found as an attachment. The final images include observations of the following times: 09:10, 09:25, 09:35, 09:40, 09:45, 09:50, 09:55. The missing observations were discarded due to poor UV coverage or corrupted files.

Our overall conclusion, is that the images are well cleaned since the rms globally decreases and the SNR increases (Figure 7). Moreover, the polarizaion calibration decreased the noise even when an IQUV calibration was used on a the Stokes I model. This is further supported by the matching of the observed flux and noise with the expected one as can be seen from Equations 2 for the Sun's signal and 3 for the thermal noise when compared with the cleaned images in Table 2.

Future plans

A more updated bandpass calibrator would result in a better calibration for the images since the ionosphere changes constantly during the day. Therefore, a model few days old does not take that into account. Another improvement of the current cleaning procedure would be taking into the account the absolute size and location of the Moon and sun on sky to create a better mask for the cleaning. Additionally, no solar phenomena such as solar flares, Coronal mass ejections or very bright spots were taken into account for the calibration and/or the expected signal/noise calculations.

Finally, the calibration of the diffraction originated from the mountains of the lunar surface, shall be calculated and calibrated out of our images.

Appendix A Additional Figures

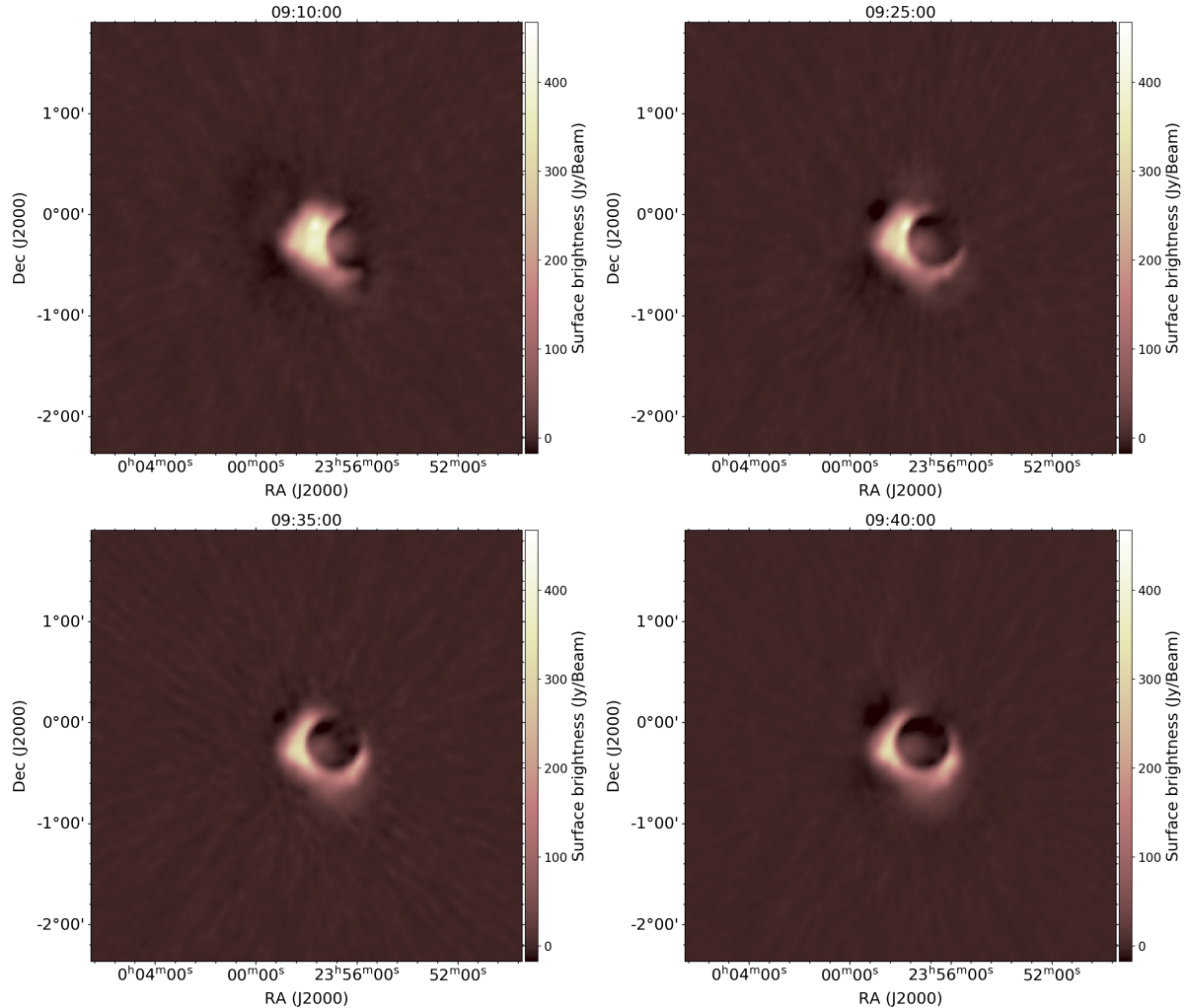


Figure 12: Final image of observations: 09:10, 09:25, 09:35, 09:40.

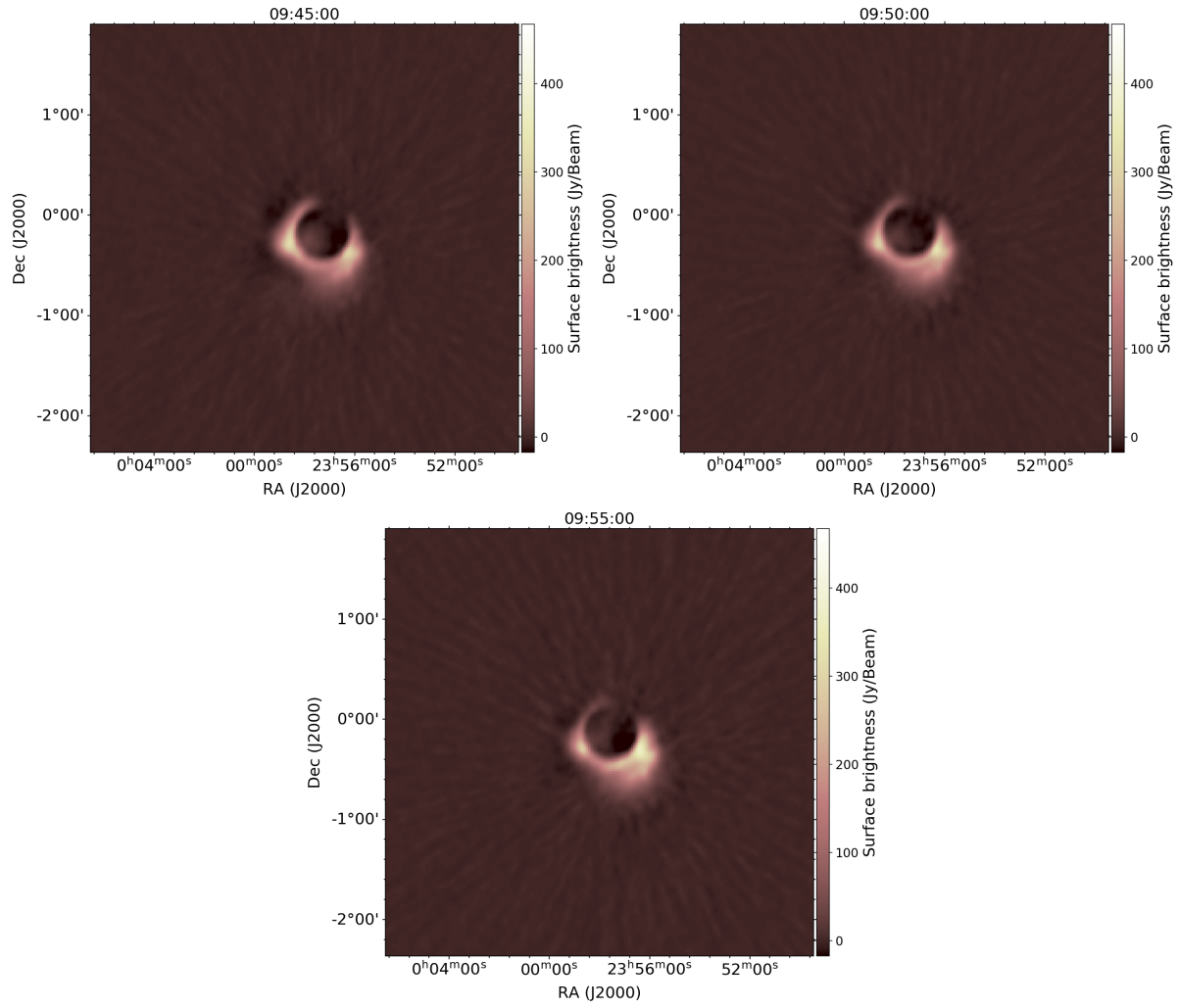


Figure 13: Final image of observations: 09:45, 09:50, 09:55

Appendix B Code

```
1 import numpy as np
2 import glob
3 import os
4 import sys
5
6
7 path= './'
8 folders_bandpass=path+'???:???:0.ms'
9 folders=path+'???:???:00'
10 folders_list=sorted(glob.glob(folders))
11 folders_list_bandpass=sorted(glob.glob(folders_bandpass))
12 refant='CS011HBA1'
13
14 '''
15 *** uncomment this part to prepare the dataset for the cleaning and comment the
16 → cleaning part ***
17
18 for fol in folders_list[:]:
19     #print(fol)
20     images= fol+'*.MS'
21     imagelist=sorted(glob.glob(images))
22     #print(imagelist)
23     print('Doing folder'+fol)
24
25     concat(vis=imagelist, concatvis=fol[2:-1]+'.ms')
26
27 for fol in folders_list_bandpass[1:]:
28     print('Doing folder'+fol)
29
30     bandpass(vis=fol, caltable=fol[:-3]+'.bandpass', refant=refant,
31 ←      gaintable='cyg-a-bandpass.cal')
32     applycal(vis=fol, gaintable='cyg-a-bandpass.cal')
33
34 for fol in folders_list_bandpass[1:]:
35     print('Doing folder'+fol)
36     badspw='7,9,18,20,27,28,29'
37     flagdata(vis=fol, mode='manual', spw=badspw)
38
39 '''
40
41 cell='1arcmin'
42 size = 256
43 nmax = 10000
44 wpp= -1
45 scale = [0,1,2,4,8,16,32,64]
```

```

46
47 basevis='07:50:0.ms'    #change this everytime for the requested dataset
48 image_folder='images_natural_'+basevis[:-3]
49
50 if not os.path.exists(image_folder):
51     os.makedirs(image_folder)
52 path_images = image_folder+'/'
53
54 def cleaning(vis, i):
55
56     if i-1 == 0:
57         automask = ''
58     else:
59         #upload the most updated mask
60         automask = path_images+'image_'+str(i-1)+'.mask'
61
62 #from image 5 onwards we create IQUV image to then solve for polarization leakage
63 if i>=5:
64     stoks='IQUV'
65 else:
66     stoks='I'
67
68 tclean(vis=basevis, imagename=path_images+'image_'+str(i), deconvolver='mtmfs', \
69         interpolation="linear", niter=nmax, scales=scale, interactive=True,
70         mask=automask,\ 
71         imsize=size, cell=cell, stokes=stoks,
72         weighting='natural',robust=-1, nterms=3,\ 
73         gridded='wproject',wprojplanes=wpp, savemodel='modelcolumn')
74
75 def selfcal(vis, i, time, mode, interptab,table='cyg-a-bandpass.cal'):
76     gaincal(vis=basevis,caltable=path_images+vis[:-2]+'_selfcal_'+str(i), solint=time,\ 
77             refant=refant, gaintype="G",calmode=mode,\ 
78             gaintable=table,interp=interptab)
79
80 # PHASE ONLY
81 j = 1
82
83 print "Cleanining: " + str(j)
84 cleaning(basevis, j)
85
86 print "Self-Cal #" + str(j)
87 selfcal(basevis, j, '0.75', 'p', '')
88
89
90 #SECOND PHASE ONLY
91 j = 2
92
93

```

```

94 print "Cleaning :" +str(j)
95 cleaning(basevis, j)
96
97
98 print"Self-Cal "+str(j)
99 selfcal (basevis, j, '0.5s','p','')
100
101 # AMP AND PHASE
102 j = 3
103
104
105 print "Apply Self-Cal " + str(j-1)
106 applycal(vis=basevis, gaintable=[path_images+basevis[:-2]+'selfcal_'+str(j-1),
107   ↵ 'cyg-a-bandpass.cal'], interp=['linear','linear'], calwt=[False], flagbackup=True)
108
109 print "Cleanining " + str(j)
110 cleaning(basevis, j)
111
112 print "Self-Cal " + str(j)
113 selfcal(basevis, j, '0.5s', 'ap','linear')
114
115
116
117 # SECOND AMP AND PHASE
118 j = 4
119
120 print "Apply Self-Cal #" + str(j-1)
121 applycal(vis=basevis,
122   ↵ gaintable=[path_images+basevis[:-2]+'selfcal_'+str(j-1), 'cyg-a-bandpass.cal'],
123   ↵ interp=['linear','linear'], calwt=[False], flagbackup=True)
124
125 print "Cleanining " + str(j)
126 cleaning(basevis, j)
127
128 print "Self-Cal " + str(j)
129 selfcal(basevis, j, '0.25s', 'ap','linear')
130
131 # Apply calibrations
132 j = 5
133
134
135 print "Apply Self-Cal #" + str(j-1)
136 applycal(vis=basevis,
137   ↵ gaintable=[path_images+basevis[:-2]+'selfcal_'+str(j-1), 'cyg-a-bandpass.cal'],
138   ↵ interp=['linear','linear', 'linear'], calwt=[False], flagbackup=True)

```

```

138 # first IQUV
139 print "Cleanining " + str(j)
140 cleaning(basevis, j)
141
142 print "Self-Cal " + str(j)
143 selfcal(basevis, j-1, '0.25s', 'ap','linear')
144
145 #I export the fits of the image
146 exportfits(imagename=+path_images+'image_'+str(j),
147             fitsimage=basevis[:-3]+'_final_image.fits')
148
149 #Final image with polarization calibration
150 j = 6
151
152 print "Pol-cal " + str(j)
153 polcal(vis=basevis, caltable=path_images+'polato.pcal', poltype='Df',
154         gaintable=['cyg-a-bandpass.cal', path_images+basevis[:-2]+'_selfcal_5',
155         path_images+basevis[:-2]+'_selfcal_2'])
156
157 print "Apply Self-Cal #" + str(j-1)
158 applycal(vis=basevis,
159           gaintable=[path_images+basevis[:-2]+'_selfcal_5','cyg-a-bandpass.cal',
160           path_images+'polato.pcal'], interp=['linear','linear', 'linear'], calwt=[False],
161           flagbackup=True)
162
163 #Second IQUV
164 print "Cleanining " + str(j)
165 cleaning(basevis, j)
166
167 #Export the fits of the image
168 exportfits(imagename=path_images+'image_'+str(j)+'.image.tt0',
169             fitsimage='IQUV'+basevis[:-3]+'_final_image.fits')

```

References

1. VAND, V. Temperature of the Solar Corona. *Nature* **151**, 728–728. <https://doi.org/10.1038/151728a0> (1943).
2. McMullin, J. P., Waters, B., Schiebel, D., Young, W. & Golap, K. in *Astronomical Data Analysis Software and Systems XVI ASP Conference Series, Vol. 376, proceedings of the conference held 15-18 October 2006 in Tucson, Arizona, USA. Edited by Richard A. Shaw, Frank Hill and David J. Bell.*, p.127 (eds Shaw, R. A., Hill, F. & Bell, D. J.) 127 (2007).
3. Rau, U. & Cornwell, T. J. A multi-scale multi-frequency deconvolution algorithm for synthesis imaging in radio interferometry. *Astronomy & Astrophysics* **532**, A71. ISSN: 1432-0746. <http://dx.doi.org/10.1051/0004-6361/201117104> (July 2011).
4. Brentjens, M. A. in *Low Frequency Radio Astronomy and the LOFAR Observatory: Lectures from the Third LOFAR Data Processing School* (eds Heald, G., McKean, J. & Pizzo, R.) 159–178 (Springer International Publishing, Cham, 2018). ISBN: 978-3-319-23434-2. https://doi.org/10.1007/978-3-319-23434-2_10.